# SPS Dipole Multipactor Test and TE Wave Diagnostics

F. Caspers, P. Costa Pinto, P. Edwards, S. Federmann, M. Holz, M. Taborelli
CERN, Geneva, Switzerland

*Abstract*

Electron cloud accumulation in particle accelerators can be mitigated by coating the vacuum beam pipe with thin films of low secondary electron yield (SEY) material. The SEY of small coated samples are usually measured in the laboratory. To further test the properties of different coating materials, RF-induced multipacting in a coaxial waveguide configuration can be performed. The technique is applied to two main bending dipoles of the SPS, where the RF power is fed through a tungsten wire stretched along the vacuum chamber (6.4 m). A dipole with a bare stainless steel chamber shows a clear power threshold initiating an abrupt rise in reflected power and pressure. The effect is enhanced at RF frequencies corresponding to electron cyclotron resonances for given magnetic fields. Preliminary results show that the dipole with a carbon coated vacuum chamber does not exhibit any pressure rise or reflected RF power up to the maximum available input power. In the case of a large scale coating production this technique will be a valuable resource for quality control. In parallel, electron cloud measurements via the microwave transmission method have been performed during the annual scrubbing run in the SPS. Clear electron cloud signals have been observed while operating with high intensity beams, confirming that this measurement technique provides a valuable tool for in-situ diagnostic. This paper is divided into two parts, where the first part deals with the multipacting test stand on stand-alone dipoles and the second part deals with the TE wave diagnostics in the CERN SPS.

## INTRODUCTION

During summer 2011, a multipacting test stand using stand-alone SPS dipoles (6.4 m) was established and commissioned. This set-up provides the possibility to check the efficiency of different carbon coatings in single coated SPS chambers under laboratory conditions. Furthermore, it can serve as quality control in the event of a large scale coating process to check the dipoles before being inserted into the machine. In 2010 and 2011, electron cloud measurements via the microwave transmission method were able to verify the coatings' performance under real beam conditions. These measurements were continued in 2012 during the annual scrubbing run.

## PART 1 - MULTIPACTING TEST STAND

### *Goal of the Test Stand*

The goal of the test stand is to induce multipacting intentionally in order to see the electron cloud build-up in stand-alone carbon-coated[1] and uncoated SPS chambers. This experiment has to fulfill the following requirements:

- Providing quality control for different carbon coatings
- Independence from the real beam and thus, independent from the accelerator's schedule
- Providing laboratory conditions

### *Experimental Set-Up*

The set-up is based on a tungsten wire, stretched inside the vacuum chamber in SPS dipole magnets. The wire and the chamber wall form a coaxial wave guide, where TEM waves can propagate[2, 3]. The far end of the wire is short-circuited. This means that injected RF power gets reflected and the dipole in the coaxial configuration intentionally works as resonator, generating a standing wave pattern with respect to the used RF frequency. As signal generator, a Rohde & Schwarz vector network analyzer (VNA) is used to perform a power ramp on a continuous wave, which is one of the set-up's resonances given by the chamber's geometry. After amplification of the generator signal, the maximum output power reaches up to 30 W - 40 W. The injected RF power provokes multipacting inside the chamber at certain locations with respect to the standing wave pattern. This set-up relies on the standing wave pattern in order to achieve the necessary electric field strength, since input power is limited by the saturation of the power amplifier. In the event of multipacting and the resulting electron cloud, power is reflected due to the free electrons in a plasma. For diagnostic purposes thus, a small fraction of the reflected power wave is coupled out by a directional coupler and transmitted to the second port of the VNA, where it is compared to its output power (without amplification). In addition, vacuum diagnostics are used to observe the symptoms, caused by electron cloud, like outgassing by electron-stimulated desorption of gas molecules and the subsequent pressure rise. The residual gas composition is monitored by a Prisma QMS200 residual gas analyzer, whilst pressure is monitored using a Pfeiffer IKR270 cold cathode gauge. A block diagram of the experimental set-up is shown in fig. 1.

### *Characterization of the stainless steel chamber*

During the commissioning of the set-up and the first tests in low magnetic fields on the bare stainless steel chamber, a pronounced outgassing and reflected power was observed. This was related to cyclotron resonance (28 GHz/Tesla), which permits to transfer energy from the RF field to the electrons in a particularly efficient manner (high scattering cross-section). The cyclotron frequency is given by eq. 1

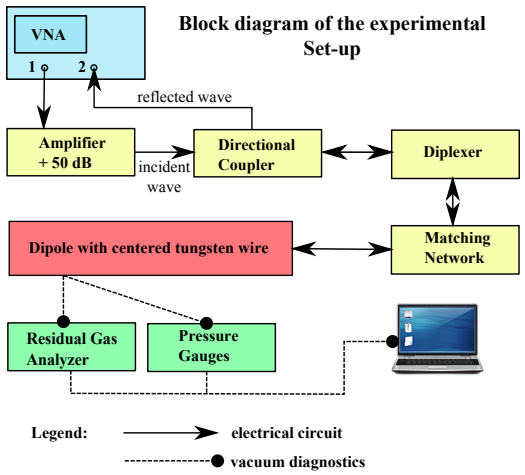


Figure 1: Block diagram of the experimental set-up. Electrical circuit and power diagnostics (beige), dipole (red) and vacuum diagnostics (green) are shown.

$$f = \frac{|q| \cdot B}{2\pi \cdot m_e} \tag{1}$$

where q is the elementary charge, B the magnetic flux density and $m_e$ the mass of the electron. A power injection frequency of around 130 MHz was used. This resonance was chosen because no matching network was required. The corresponding magnetic flux density in order to reach cyclotron resonance calculates to 4.6 mT. Using the transfer function of a reference dipole, it is possible to relate applied electric currents to the magnetic field, generated by the dipole. It turns out that for achieving a magnetic field of 4.6 mT, a current of roughly 11 Ampere has to be fed into the magnet. In order to verify the pronounced effect at cyclotron resonance, measurements were performed as a function of magnetic field in the region around 4.6 mT and reflected power as well as outgassing was monitored during these tests. Figure 2 shows the outgassing due to the electron-stimulated desorption as a function of varying currents through the magnet and figure 3 shows the corresponding reflected power.

The base line levels showed in fig. 3 are slightly different and depend on the coupling between the electrical circuit and the resonator. The differences are due to minor mismatches, caused by thermal drift of the wire during the measurements. The minimum of the multipacting threshold corresponds well to the magnetic field value calculated for this frequency. A series of experiments was performed with two different RF frequencies to prove unambiguously the effect of the cyclotron resonance. The main desorbed gases are $H_2$, $CO$ and $CO_2$, which makes them representative for the residual gas analysis. Water, the dominant gas in static conditions, does not exhibit a significant rise in outgassing during the multipacting event. The significant rise in carbon monoxide and carbon dioxide, however, is a clear fingerprint of electron-stimulated desorption in contrast to the mostly thermal outgassing of water. Un-

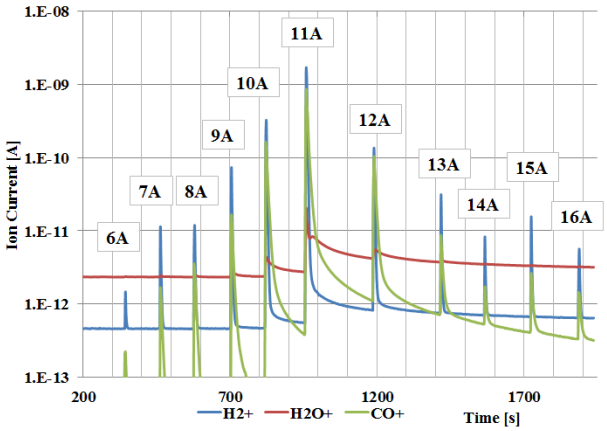


Figure 2: Outgassing for hydrogen, water and carbon monoxide at different magnetic fields with a pronounced maximum around the calculated resonant condition (10.8A).

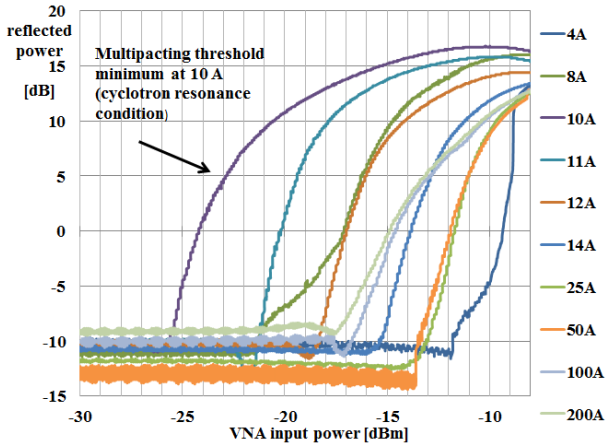


Figure 3: Reflected power, measured in the low magnetic field range on the uncoated chamber.

der cyclotron resonance condition, a glow discharge in the blue visible (and possibly ultra-violet) spectrum could be observed through a small viewport.

Figure 4 shows the observed plasma. Cyclotron resonance strongly enhances the sensitivity to changes in the surface properties and amplifies the observable differences between stainless steel and carbon coated surfaces and thus, clearly enhances this measurement method to a stress test of carbon coatings. Several arguments that could explain the lower threshold of reflected power and the higher pressure rise at cyclotron resonance are discussed below. Due to the resonance, the electrons gain a larger energy in the direction tangential to the surface of the beam pipe. Thus the multipacting electrons at higher energy could be more effective for electron-stimulated desorption. In addition the electrons impact on the surface at a larger incidence angle (with respect to the surface normal) and result in a higher secondary electron yield. With the current set-up it is difficult to disentangle the two effects. Figure 5

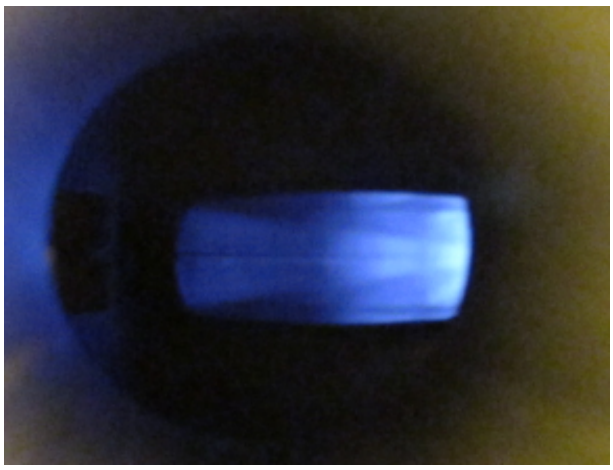

Figure 4: Evidence of plasma formation by emitted light in the blue visible (and possibly ultra-violet) spectrum. Observable only under cyclotron resonance.

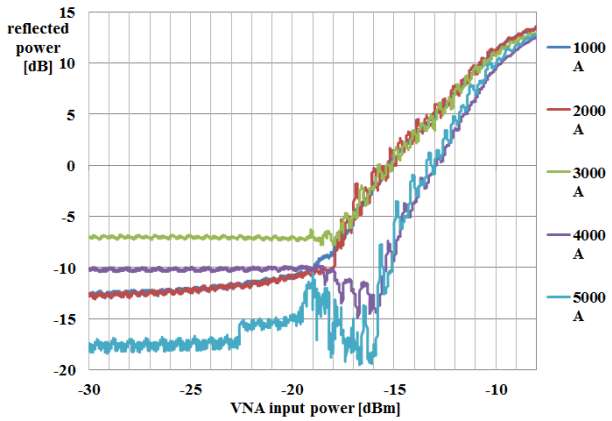


Figure 5: Reflected power, measured in the high magnetic field range on the uncoated chamber.

shows the reflected power for measurements at high magnetic fields, where the electrons are expected to be confined along the magnetic field vector. In this magnetic field region, the threshold for the multipacting onset is almost independent of the field. Small modulating oscillations on the traces are due to mechanical vibrations of the wire caused by e.g. the pumping system.

### *Results of the magnetron-sputtered Coating*

After the inner surface of the chamber was fully coated by magnetron sputtering, tests at 130 MHz and as a function of magnetic field have been repeated. Generally, no reflected power and no outgassing/pressure rise was observed, even at cyclotron resonance. This indicates that the coating does not just reduce multipacting, but completely suppresses it for the provided input power. One exception occurred at the first measurement feeding 3000 A through the magnet. There, a sharp rise in reflected power was observed. Also, pressure has risen strongly during this event. Having repeated this test with 3000 A (= 1.14 T) no reflected power could be observed, however, pressure activity remained for all consecutive measurements, including repeated measurements in the low magnetic field region. As it seems that something was "activated", the reason for this is still not fully understood. One assumption is that the multipacting took place at another location inside the multipacting system, for example at or near the pumping port, the bellows at the beginning and the end of the dipole or the pre-chamber, which houses the device to attach the wire and the conductances to the vacuum diagnostics. Figure 6 shows the reflected power for the coated chamber and figure 7 shows the corresponding pressure data, including the pressure for the uncoated chamber to compare.

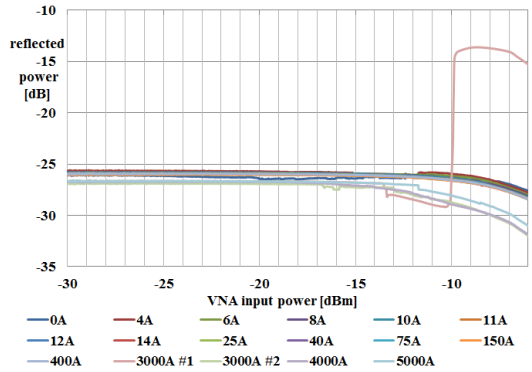


Figure 6: Reflected power from the coated chamber. A single increase for the first measurement with 3 kA occurred. Decreasing signal levels towards the end of the power sweep are due to the compression of the power amplifier.

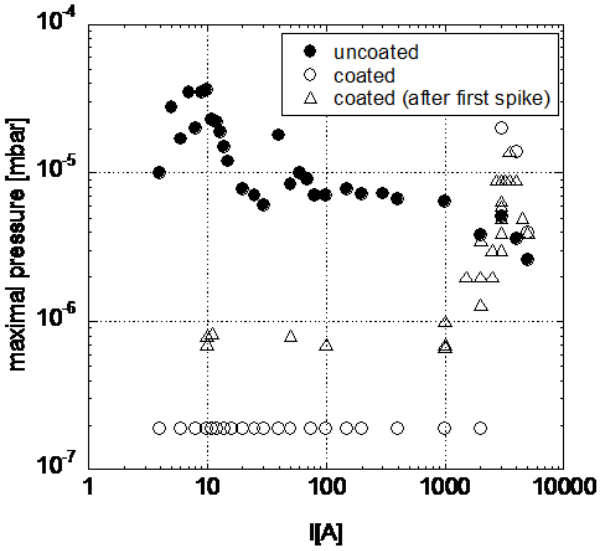


Figure 7: Pressure data for the uncoated (black dots) and the coated (white dots) chamber. Remanent pressure activity after the exceptional multipacting event (white triangles).

## PART 2 - TE WAVE DIAGNOSTICS IN THE CERN SPS

### *Goals of the Microwave Transmission Measurements*

Firstly, the main goal of the e-cloud measurements by means of microwave transmission is to provide an in-situ diagnostic tool to check the carbon coatings under real beam conditions when inserted in the SPS. Furthermore, it serves as on-line diagnostic tool to measure the integrated electron cloud density during the annual scrubbing run and machine development. Further development could possibly include also the on-line estimation of the average e-cloud density in number of particles per square meter.

### *Measurement Principle*

The principle of this method is the analysis of the phase modulation (PM) of an injected continuous wave which serves as carrier wave in the set-up. The phase shift of the carrier wave is induced by passing a plasma-filled waveguide. In the case of an accelerator, the plasma is the electron cloud. The phase shift is given by equation 2[4]:

$$\begin{aligned}\Delta\varphi &= \frac{L\omega_p^2}{2c(\omega^2-\omega_c^2)^{\frac{1}{2}}} \\ &= \frac{L\sqrt{\frac{n_e e^2}{\epsilon_0 m_e}}^2}{2c(\omega^2-\omega_c^2)^{\frac{1}{2}}} \\ &\cong \frac{L\cdot 3181 n_e}{2c(\omega^2-\omega_c^2)^{\frac{1}{2}}}\end{aligned} \tag{2}$$

where $\omega$ is the injected frequency, L the transmission length, $\omega_c$ the cutoff frequency of the waveguide, c the speed of light, $\omega_p$ the plasma frequency, $\epsilon_0$ the permittivity in free space,e the electron charge, $m_e$ the electron mass and $n_e$ the number of electrons per square meters. Note that this equation assumes a nearly lossless transmission, which means no internal and external reflections, causing resonances. Since the beam cycles many times in the machine whilst recording, the integrated electron cloud density is measured. Equ. 2 shows that the phase shift encountered by the carrier wave is directly proportional to the electron cloud density. All other parameters are usually known.

### *Experimental Set-up and Results 2011*

In 2010 and 2011, the set-up was used to measure two SPS bending dipoles, inserted in the machine, where one of them was coated with a thin layer of amorphous carbon (200nm - 300 nm) [5]. The second, uncoated dipole served as reference allowing direct comparison of the obtained results. The carrier wave was coupled in between these two dipoles and signal pick-ups were installed upstream and downstream at their ends. Figure 8 shows the set-up scheme as it was used in 2011 and figure 9 shows part of the spectrum of the beam and the modulated carrier wave as it appears on the screen of the vector spectrum analyzer.

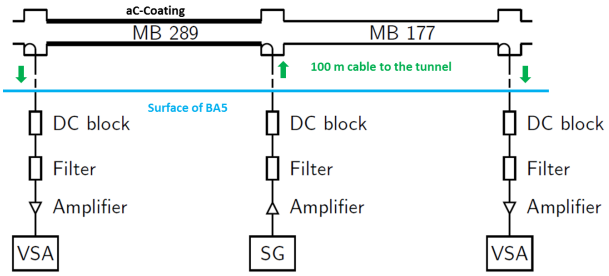


Figure 8: Schematic layout of the SPS microwave transmission measurement with a coated chamber (MB 289) and an uncoated chamber (MB 177) as it was used in 2011. VSA: vector spectrum analyzer, SG: signal generator. [S. Federmann]

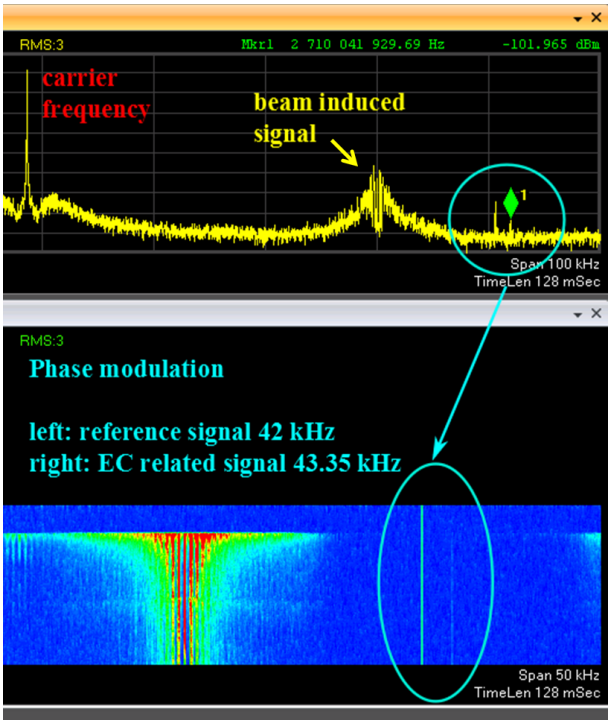


Figure 9: Top: Spectrum of a recent sample measurement. The electron cloud (EC) signal is marked and accompanied by a PM reference signal. Bottom: Phase-demodulated spectrum in spectrogram mode. Batch injection can be seen via the beam induced signals.

In the frequency domain the modulation appears in sidebands, located at the positive and negative distance of the modulation frequency from the centered carrier frequency. In the case of the SPS, the phase modulation occurs at the revolution frequency of 43.35 kHz (23 $\mu s$). In the spectrogram, it can be seen that the electron cloud induced signal

is related to the batch injection, which is indicated by the onset of the beam induced signals. In 2011, data was taken at nominal LHC 25 ns beam, four batches and flat bottom. While in the uncoated dipole, a clear electron cloud induced phase shift was detected, the coated dipole did not exhibit a detectable phase shift.

### *Set-Up 2012*

During the annual scrubbing run in 2012, one of the main interests was to check the feasibility of the microwave transmission measurements to measure a longer section of the SPS. First measurements were performed measuring two consecutive uncoated SPS MBB magnets. Additionally, it was observed whether the conditioning of the surface due to the scrubbing is detectable by this set-up or not. A scheme of the set-up is shown in fig. 10:

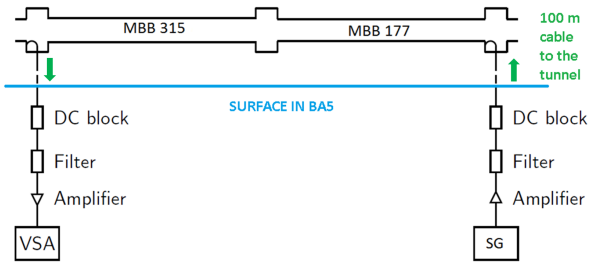


Figure 10: Schematic layout of the SPS microwave transmission measurement with two uncoated chambers as it was used in 2012. VSA: vector spectrum analyzer, SG: signal generator. [S. Federmann]

### *Results 2012*

During these measurements, the signal generator injected a 10 dBm carrier wave of 2.71 GHz which was at a maximum in transmission according to the hardware transfer function. As calibration signals, either a phase modulation with 1 mrad or an amplitude modulation with 1 % of the carrier amplitude was applied with a frequency of 42 kHz. For evaluation of the data both frequencies, the calibration signal and the phase-modulated electron cloud signal are filtered by software from the recordings and displayed versus time. Measurements were taken with a vector spectrum analyzer which had a rather small size of internal memory which limited the recording time to 8 seconds. Thus, recording the complete supercycle of the beam was impossible and it has been triggered manually just before the injection of the last batches. Figure 11 shows a measurement for the empty machine after a beam dump. The PM base level for the electron cloud signal is at $-71\ dB$ compared to 1 rad. For all subsequent measurements this is considered as reference level. The calibration signal shows an average level of -60 dB which matches the preset 1 mrad from the signal generator.

Figure 12 shows the results for a beam with 4 batches,

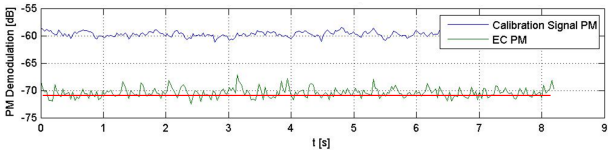


Figure 11: Time trace of the electron cloud induced signal (EC) and the calibration signal for an empty machine. Obtained average base level is around -71 dB (red line).

25 ns spacing and a maximum total intensity of $3455{\cdot}10^{10}$ protons. In this measurement a small increase in phase modulation can already be noticed. The depicted trace was recorded after the injection of the fourth batch. Compared to the reference level we obtained above, one can see that the e-cloud signal has risen 4 dB up to -67 dB. This signal was completely reproducible for the following beams and the same beam parameters.

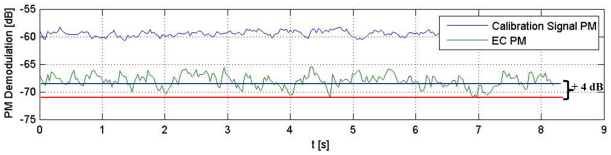


Figure 12: Time trace of an increased electron cloud induced signal around $-67\,dB$. +4 dB compared to reference level. 4 batches, 25 ns spacing and a maximum total intensity of $3455{\cdot}10^{10}$ protons. Recorded after injection of the fourth batch.

During the scrubbing run the vector spectrum analyzer was replaced with a more recent version with a larger internal memory. Thus, it was possible to record complete supercycles and the manual trigger was not necessary anymore. According to the data sheets, the two spectrum analyzers are indeed equal in terms of sensitivity and accuracy. Therefore, all taken measurements are directly comparable. Subsequently, the dynamic behavior of the e-cloud signal could be observed. For the measurement shown in fig. 13, the beam parameters were one batch, 25 ns spacing and a maximum total intensity of $1274{\cdot}10^{10}$ protons. Taking a look at the time traces, one can see a very slight increase at 18 seconds in electron cloud phase modulation which is an indication that an electron cloud is present (red box). This occurs simultaneously with batch injection. Batch injections can be identified by spikes in the amplitude-demodulated part. The previous signals in this time trace are due to the presence of a low intensity beam.

In the case of two batches, the results with 25 ns spacing and a maximum total intensity of $2530{\cdot}10^{10}$ protons for the high intensity beam (fig. 14, red box) are shown. At 32 seconds, where the second batch injection took place, a clear step in PM can be seen. Since we measure the in-

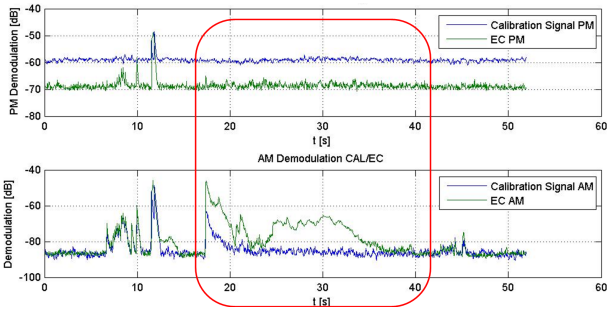


Figure 13: High intensity beam (red box): One batch, 25 ns spacing and a maximum total intensity of $1274{\cdot}10^{10}$ protons. Small increase in e-cloud PM signal since batch injection at 18 seconds (top). Batch injection can be identified by spikes in AM (bottom).

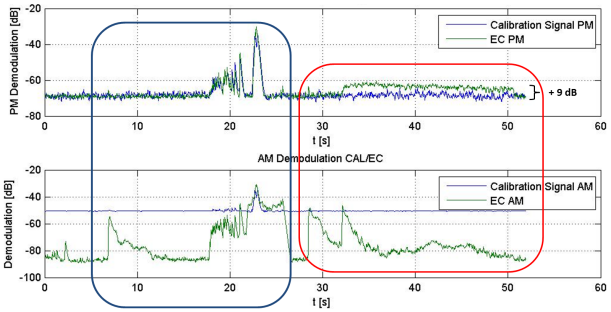


Figure 14: Clear step in PM e-cloud signal after the second batch of the high intensity beam at 32 s (top). Injections visible in AM part (bottom). High intensity beam (red box): Two batches, 25 ns spacing and a maximum total intensity of $2530{\cdot}10^{10}$ protons. Low intensity beam (blue box): One batch, 25 ns spacing and a maximum total intensity of $871{\cdot}10^{10}$ protons (no e-cloud). Measurement direction was upstream.

tegrated electron cloud density, this rise is related to the longer and also more dense presence of electron cloud due to two consecutive batches, accumulated over many beam cycles in the ring. The magnitude of phase modulation after injection of the second batch can be extracted from the time trace and gives roughly $-62\,dB$, which is $+9\,dB$ with respect to the reference level at $-71\,dB$. The previous signals (fig. 14, blue box) are due to an injection and an acceleration of a low intensity beam with one batch, 25 ns spacing and a maximum total intensity of $871{\cdot}10^{10}$ protons. One can see that the spectrum anaylzer is dazzled by the changing RF due to beam acceleration. During the presence of the this beam, no e-cloud could be observed. Note, that for this measurement an AM calibration signal was applied and thus, it appears in the AM part. Also, a weak signal at the calibration signal frequency (42 kHz) in PM was observed. It cannot be seen well in the time traces for it is almost indistinguishable from the background. This indicates a slight AM to PM conversion, which is probably due to some slope in the hardware transfer function (HTF) of the measurement set-up. Unevenness in the HTF may cause different transmission coefficients for the lower side band and the upper side band, resulting in a mixture of AM and PM.

The parameters for the high intensity beam in fig. 15 are 3 batches, 25 ns spacing and a maximum total intensity of $3639{\cdot}10^{10}$ protons. The results for this measurement are as expected. An additional step in the e-cloud signal after injection of the third batch is clearly visible. For the low intensity beam with the same parameters like in the previous measurement, no electron cloud could be detected again. This measurement was performed downstream (in beam direction).

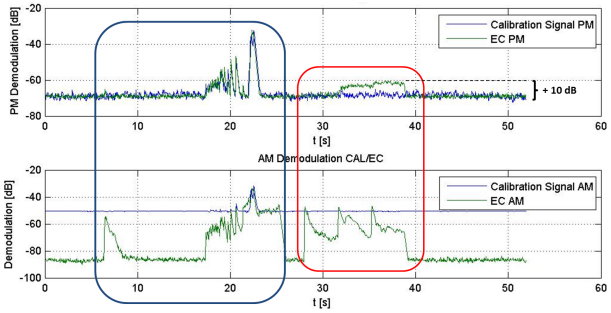


Figure 15: Clear step in e-cloud signal for the high intensity beam after second and third batch at 32 s and 35 s, respectively. High intensity beam: 3 batches, 25 ns spacing and a maximum total intensity of $3639{\cdot}10^{10}$ protons. Low intensity beam: One batch, 25 ns spacing and a maximum total intensity of $872{\cdot}10^{10}$ protons (no e-cloud). Measurement direction was downstream.

## CONCLUSION

A coaxial resonator method for multipacting tests on SPS beam pipe sections in a magnet was developed. The results in terms of multipacting threshold appear to be reproducible and consistent. Several independent diagnostic tools for multipacting were applied (vacuum, reflected RF power, light emission). At cyclotron resonance, a strong enhancement of the multipacting effect was found and thus, increasing the sensitivity of the set-up, especially when comparing the results to coated chambers. The coated magnet, even at cyclotron resonance, practically did not show any multipacting within the available power range.

The microwave transmission method proved to be feasible for measurements of two consecutive and uncoated dipoles in the SPS. Clear electron cloud induced signals in the form of a phase modulation of a carrier wave could be obtained with high intensity beams and 25 ns bunch spacing during the annual scrubbing run. For low intensity beams, no electron cloud induced phase modulation was

detected. During the acceleration of the beam, the vector spectrum analyzer is dazzled by the changing RF. Thus, only measurements at flat top and flat bottom are useful. The measurements were performed upstream and downstream, but no asymmetry was found. The current set-up does not require any active electronics in the tunnel, which could otherwise be damaged by radiation. The new vector spectrum analyzer makes it possible to record the complete supercycle and triggering manually is obsolete. Additionally, it is possible for future measurements to increase the resolution bandwidth from 100 kHz to 1 MHz and to include the first few harmonics of the e-cloud induced modulation in order to get the time-resolved electron cloud build-up.

## ACKNOWLEDGMENT

We would like to thank the management of TE and BE departments and our group leaders J.M. Jimenez, TE-VSC group and E. Jensen, BE-RF group for supporting this project. Many thanks to Reinier Louwerse for providing the power amplifier for the multipacting test stand and to Michael Betz for providing the new vector spectrum analyzer.

## REFERENCES

[1] C. Yin Vallgren et al., *"Low Secondary Electron Yield Carbon Coatings For Electron Cloud Mitigation In Modern Particle Acclerators"*, WEOAMH03,IPAC'10, Kyoto, Japan.

[2] F. Caspers, J.-M. Laurent, M. Morvillo, and F. Ruggiero, *"Multipacting tests with a resonant coaxial setup"*, CERN, LHC Project Note 110, 1997.

[3] U. Iriso, F. Caspers, J-M. Laurent, and A. Mostacci, *"Traveling wave resonant ring for electron cloud studies"*, Phys. Rev. Special Topics - Accelerators and Beams,Volume 7, 073501 (2004)

[4] S. De Santis, J. M. Byrd, F. Caspers, A. Krasnykh, T. Kroyer, M. T. F. Pivi and K. G. Sonnad, *"Measurement of Electron Clouds in Large Accelerators by Microwave Dispersion"*, Phys. Rev. Lett. Vol.100, 094801 (2008)

[5] S. Federmann, F. Caspers, and E. Mahner, *"Measurements of electron cloud density in the CERN Super Proton Synchrotron with the microwave transmission method"*, PHYSICAL REVIEW SPECIAL TOPICS - ACCELERATORS AND BEAMS, Volume 7, 012802 (2011)